Catalysis Science & Technology

ROYAL SOCIETY OF CHEMISTRY

PAPER

View Article Online
View Journal | View Issue

Cite this: *Catal. Sci. Technol.*, 2025, **15**, 5335

Correlating electronic properties of a nickel polymerisation catalyst with the branching density of a polyethylene

Yifan Zeng, [a] Yizhou Wang, [b] Kuldip Singh,[a] Gregory A. Solan, *[ab] Yanping Ma [b] and Wen-Hua Sun *[b]

Received 14th July 2025,
Accepted 12th August 2025

DOI: 10.1039/d5cy00859j

rsc.li/catalysis

This work investigates how the electronic properties of a nickel ethylene polymerisation catalyst can be used to exert control on key polymerisation steps namely chain walking and chain propagation and in turn affect branching and polymer molecular weight. Specifically, a series of sterically enhanced 2-(imino)-4-R-pyridine–nickel complexes (R = OMe **Ni1**, Me **Ni2**, H **Ni3**, Br **Ni4**, CF_3 **Ni5**, NO_2 **Ni6**) that differ only in the electronic properties of the *para*-R substituent have been prepared and fully characterised. Under activation with EASC (ethyl aluminium sesquichloride), all nickel catalysts exhibited high activities for ethylene polymerisation and produced branched polyethylenes (BPE: branching density range: 61–99/1000 Cs) with a range of molecular weights (4.89–15.4 kg mol^{-1}); the relative order of catalytic activity being: **Ni5** (CF_3) > **Ni4** (Br) > **Ni1** (OMe) > **Ni6** (NO_2) > **Ni3** (H) > **Ni2** (Me). Additionally, cyclovaltametry measurements performed on **Ni1–Ni6** have been used to measure half-wave potentials ($E_{1/2}$) that can serve as a quantitative descriptor of the electronic effect. Moreover, good correlations exist between $E_{1/2}$ and i) the degree of branching and ii) the polymer molecular weight. Importantly, this study highlights the potential of $E_{1/2}$ as a predictive tool for rational design of catalysts to make tailored BPE's.

Introduction

Polyethylene is a commercially important polymer that is considered as the most widely produced polyolefin globally.[1–4] As a significant variant of it, branched polyethylene (BPE) has been utilised in a broad range of industrial and bioengineering applications and fields including films, sensors, capsules as well as end-uses exploiting their elastomeric properties (POEs).[5–15] Traditionally, the production of BPE's have relied on either a high pressure free radical process or a metal-catalysed copolymerisation process.[1,16–19] As an alternative approach, a metal-mediated polymerisation process making use of ethylene as the sole feedstock offers an attractive and direct route to such valuable polymers.

In this regard nickel-based catalysts bearing α-diimine *N*,*N*-chelating ligands (*e.g.*, 1,4-diazabutadiene, 2-iminopyridine *etc.*) have emerged over the last 30 years that can mediate the formation of BPE's *via* a distinctive chain-walking process.[20–24] Indeed a wide range of branched architectures are accessible that can be influenced by not only physical properties such as temperature and pressure but also by the structural properties of the catalyst.[25–27]

In terms of the catalyst structure, electronic and steric changes made to the *N*,*N*-ligand manifold have proved highly influential whereby distinct effects can be observed on catalyst activity, polymer molecular weight and the branching properties of the PE.[4,5,28] With respect to steric variations, the introduction of exceptionally bulky groups to the *ortho*-positions of the *N*-aryl groups such as benzhydryl ($CHPh_2$), represents a more recent approach that has seen increases in polymer molecular weight (M_w), branching content as well as thermal stability of the catalyst (*e.g.*, **I**, in Chart 1).[29]

Elsewhere electronic changes to the remote *para*-positions of the *N*-aryl groups have been studied on a range of *N*,*N*-ligand frames (*e.g.*, **I** and **II**, Chart 1).[30,31] For *N*,*O*-chelated nickel precatalysts, Chen *et al.* found that such electronic perturbations can play a role in determining the polyethylene branches (**III**, Chart 1).[32] Similarly, Long *et al.* studied electronic effects made to the backbone and *N*-aryl group in **IV** (Chart 1) and additionally reported some correlation between the redox half-wave potential ($E_{1/2}$) of the particular *N*,*N*-nickel precatalyst and the observed polyethylene branching.[33]

[a] *Department of Chemistry, University of Leicester, Leicester LE1 7RH, UK. E-mail: gas8@leicester.ac.uk*
[b] *Key Laboratory of Engineering Plastics and Beijing National Laboratory for Molecular Sciences, Institute of Chemistry, Chinese Academy of Sciences, Beijing 100190, China. E-mail: whsun@iccas.ac.cn*

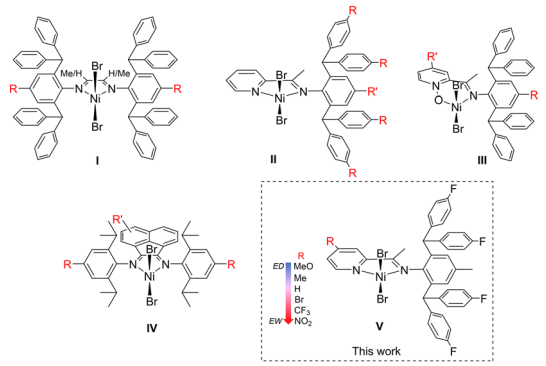

Chart 1 Selected examples of Ni(II) ethylene polymerisation precatalyst (I–IV), including this work (V), and the sites on their ligand framework (R) used to study electronic effects.

With the aim to gain a greater understanding about the relationship between $E_{1/2}$ at the catalyst level and various properties of the resulting polymers, a more diverse range of substituents with a wider range of electronic properties was targeted. Herein, we report a family of 2-(arylimino)-4-R-pyridines-nickel(II) bromide complexes each appended with an *N*-2,6-bis{di(4-fluoro)benzhydryl}-4-methylphenyl group (Chart 1). Six members of this family, differing in the electronic properties of the 4-R group (*viz.* OMe, Me, H, Br, CF_3, NO_2) on the pyridine moiety are discussed, and these precatalysts are employed under identical conditions as catalysts for ethylene polymerisation. We reasoned that by positioning the R group on the *para*-position of the pyridine donor, it would have a more significant effect on performance than in **I–IV** (Chart 1). Full details of the synthetic and polymerisation procedures are presented alongside the cyclovoltammetry measurements and various other characterisation methods.

Results and discussion

(a) Synthesis and characterisation of ligands and complexes

A series of 2-(arylimino)-4-R-pyridines, 2-{(2,6-{(*p*-FC_6H_4)$_2$-CH}$_2$-4-MeC_6H_2)N=CMe}-4-RC_5H_3N (**L1** R = OMe, **L2** R = Me, **L3** R = H, **L4** R = Br, **L5** R = CF_3, **L6** R = NO_2) were prepared by the condensation reaction of 2-acetyl-4-R-pyridine with 2,6-bis(bis(4-fluorophenyl)methyl)-4-methylaniline in moderate to good yields (Scheme 1). Subsequently, the corresponding nickel(II) complexes, [(*N*,*N*)$NiBr_2$] [*N*,*N* = **L1** (**Ni1**), **L2** (**Ni2**), **L3** (**Ni3**), **L4** (**Ni4**), **L5** (**Ni5**), **L6** (**Ni6**)] were synthesised by reacting **L1–L6** with one equivalent of $NiBr_2$(DME) (DME = 1,2-dimethoxyethane) in dichloromethane at ambient temperature. Compounds **L1–L2**, **L4–L6** and their corresponding nickel complexes are novel, while **L3** and **Ni3** have been reported before.[30] All compounds were obtained in good yield and characterised by a combination of ^{1}H, ^{13}C and ^{19}F NMR, FT-IR spectroscopy, HRMS, single crystal X-ray diffraction and elemental analysis.

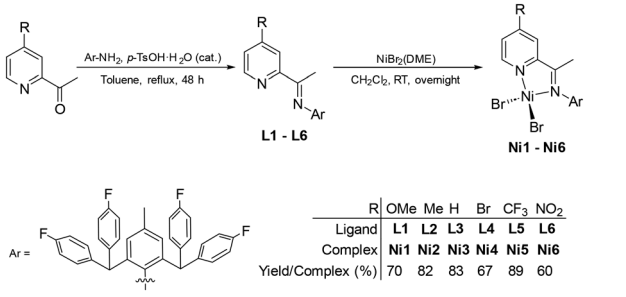

Scheme 1 Synthetic route to 2-imino-4-R-pyridines, **L1–L6** and their nickel(II) bromide complexes, **Ni1–Ni6**.

Single crystals of **Ni1**, **Ni2**, **Ni3** and **Ni4** suitable for the X-ray determinations were grown by slow cooling of hot acetonitrile solutions of each complex, while those for **Ni5** and **Ni6** were grown from dichloromethane by layering with diethyl ether or hexane. Only the structure of **Ni1** (Fig. 1) will be discussed in any detail, while crystallographic details for **Ni2** to **Ni6** are presented in the SI.

A view of **Ni1**(NCMe) is shown in Fig. 1, while selected bond lengths and bond angles are given in the caption. The structure consists of a single Ni(II) centre surrounded by *N*,*N*-chelating **L1**, two bromide ligands and a molecule of acetonitrile to complete a coordination geometry best described as distorted trigonal bipyamidal (τ_5 value[34] = 0.60). The molecule of acetonitrile derives from adventitious coordination during crystallisation.[35] The $Ni(1)–N(2)_{imine}$ bond distance of 2.0465(18) Å is slightly longer than the $Ni(1)–N(1)_{pyridine}$ of 2.0255(19) Å, which likely reflects the steric properties of the *N*-aryl group. It is noteworthy that the electronic properties of the *para*-R group have some effect on the $Ni(1)–N(1)_{pyridine}$ bond lengths when all six structures are compared (see Table S3). Notably, when the electron

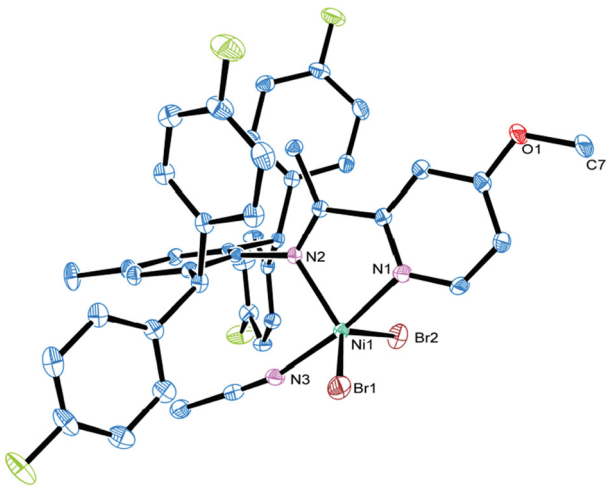

Fig. 1 ORTEP representation of **Ni1**(NCMe) with the thermal ellipsoids set at the 50% probability level; the hydrogen atoms have been omitted for clarity. Selected bond distances (Å): Ni(1)–Br(1) 2.4506(4) Ni(1)–Br(2) 2.4538(5), Ni(1)–N(1) 2.0255(19), Ni(1)–N(2) 2.0465(18), Ni(1)–N(3) 2.0373(19), selected bond angles (°): Br(1)–Ni(1)–Br(2) 135.581(18), N(1)–Ni(1)–Br(1) 90.21(6), N(1)–Ni(1)–Br(2) 89.37(6), N(1)–Ni(1)–N(2) 78.98(7), N(1)–Ni(1)–N(3) 171.33(8).

withdrawing properties of R increase, the Ni(1)–$N(1)_{pyridine}$ distance in general increases from 2.0255(19) Å in methoxy-containing **Ni1**(NCMe) to 2.0453(18) (Å) in NO_2 derivative **Ni6**(NCMe); the outlier being for **Ni3**(NCMe) (2.0493(14) (Å)). The N(2)–C(6) double bond of 1.287(3) (Å) in **Ni1**(NCMe) is typical of a C=N double bond, while the sterically bulky *N*-2,6-bis{di(4-fluoro)benzhydryl}-4-methylphenyl group is inclined towards perpendicular to the *N*,*N*-coordination plane. The $O(1)–C(3)_{pyridine}$ bond distance of 1.345(3) (Å) is distinctly shorter than that of $O(1)–C(7)_{methyl}$, 1.436(3) (Å), which indicates some π-interaction of the methoxy oxygen atom with the pyridine ring. There are no intermolecular contacts of note.

In the IR spectra of **Ni1** to **Ni6**, the $\upsilon(C{=}N)_{imine}$ absorptions fall around 1600 cm^{-1} which are typically 23–50 cm^{-1} less than that seen in **L1** to **L6**. All complexes are paramagnetic and gave magnetic moments (μ_{eff} range: 2.64–3.05 BM) that are consistent with two unpaired electrons (S = 1).[36,37] In their ^1H NMR spectra, this paramagnetism is manifested by broad and highly shifted peaks appearing in their ^1H NMR spectra (see Table S1). Typically, these peaks are seen in the range −23 to +221 ppm with some level of assignment possible. For example, the *meta*-protons belonging to the pyridine ring appear between 60–80 ppm, while the *ortho*-protons are highly downfield shifted to *ca.* 200 ppm (broad and weak). Similarly, the peaks observed in the region of 15–20 ppm and 25–30 ppm can be assigned to the *N*-aryl *meta* protons and imine-methyl protons, respectively, based on comparison with previous studies performed in our group.

Conversely, their ^{19}F NMR spectra are simpler and each reveal two distinct signals which suggests some restricted rotation for the F-substituted *ortho*-benzhydryl groups. In the case of **Ni5**, an additional more downfield fluorine resonance is seen for the *para*-CF_3 group. In their mass spectra, fragmentation peaks corresponding to $[M–Br]^+$ ions are seen for all complexes. The microanalytical data for all nickel complexes further support the proposed $LNiBr_2$ composition.

(b) Catalytic evaluation and polymer characterisation

To determine the most suitable activator, five different aluminium-alkyl reagents were initially assessed using **Ni1** as the test precatalyst (Table 1). All polymerisation runs were performed in toluene with the ethylene pressure set at 10 atm, the temperature at 30 °C and the run time at 30 min. By employing MAO (methylaluminoxane), MMAO (modified methylaluminoxane), $EtAlCl_2$, Et_2AlCl and EASC (ethyl aluminium sesquichloride), it was found that the resultant catalytic activities using **Ni1** followed the order: EASC > Et_2-AlCl > $EtAlCl_2$ > MMAO > MAO. In terms of molecular weights of the polyethylenes, it was noted the ethyl aluminium chloride containing activators tended to form slightly higher values when compared to their MAO comparators but showed slightly broader dispersities. On the basis of the level of catalytic activity, EASC was taken forward for further for more detailed studies.

To identify an effective set of conditions that could be used to evaluate all six nickel precatalysts using EASC, **Ni1** was subjected to a series of experiments directed towards ascertaining the optimal run temperature and Al : Ni molar ratio (Table 2). In the first instance, the temperature of the run using **Ni1**/EASC was varied from 20 °C to 50 °C with the Al : Ni ratio fixed at 400 : 1 (runs 1–4, Table 2). The highest activity of 1.87×10^6 g of PE (mol of Ni)$^{-1}$ h^{-1} was found at 30 °C generating a narrowly disperse polymer (M_w/M_n = 1.89) with a molecular weight of 6.14 kg mol^{-1}. In terms of variations in polymer molecular weight, a general drop was seen from 13.0 kg mol^{-1} at 20 °C to 3.09 kg mol^{-1} at 50 °C, in line with thermally induced chain transfer. Inspection of the corresponding T_m values reveals a general decrease in accordance with the lowering in M_w and also greater branching (*via* chain-walking) in the polymer as the temperature was increased (runs 1–4, Table 2). With the run temperature maintained at 30 °C, the Al : Ni molar ratio was then varied between 300 : 1 to 700 : 1 (runs 2, 5–8, Table 2) with the result that 600 : 1 gave the peak activity of 2.03×10^6 g of PE (mol of Ni)$^{-1}$ h^{-1}. Once again, the dispersity of the polymer remained narrow and the molecular weight comparable with the obtained with an Al : Ni ratio of 400 : 1 (run 2, Table 2).

With an effective set of conditions established for **Ni1**/EASC, [Al : Ni = 600 : 1, run temperature = 30 °C, $P_{C_2H_4}$ = 10 atm, run time = 30 min], the remaining five nickel precatalysts, **Ni2**–**Ni6**, were evaluated similarly (runs 9–13, Table 2). All catalysts proved highly active displaying well-controlled polymerisations (M_w/M_n range: 1.75–2.41) with their relative order being: **Ni5** (CF_3) > **Ni4** (Br) > **Ni1** (OMe) > **Ni6** (NO_2) > **Ni3** (H) > **Ni2** (Me). With the exception of **Ni6**, the nickel catalysts bearing electron-withdrawing *para*-R

Table 1 Activator screening using **Ni1** for ethylene polymerisation[a]

Entry	Activator	PE (g)	Al : Ni	Act.[b]	M_w[c]	M_w/M_n[c]	T_m[d] (°C)
1	MAO	0.79	2000 : 1	0.79	2.41	1.63	63.7
2	MMAO	1.16	2000 : 1	1.16	2.66	1.75	69.3
3	$EtAlCl_2$	1.23	400 : 1	1.23	4.62	1.85	59.8
4	Et_2AlCl	1.60	400 : 1	1.60	4.22	1.82	50.5
5	EASC	1.87	400 : 1	1.87	6.14	1.89	64.4

[a] Conditions: 2.0 μmol of **Ni1**, 100 mL of toluene, 10 atm C_2H_4, 30 °C, 30 min. [b] Values in units of 10^6 g (PE) (mol of Ni)$^{-1}$ h^{-1}. [c] M_w in units of kg mol^{-1}, determined by GPC. [d] Determined by DSC.

Table 2 Ethylene polymerisation results using **Ni1**–**Ni6** and EASC[a]

Run	Precatalyst	T (°C)	Al : Ni	Activity[b]	M_w[c]	M_w/M_n[c]	T_m[d] (°C)
1	**Ni1**	20	400 : 1	1.17	13.0	2.05	93.5
2	**Ni1**	30	400 : 1	1.87	6.14	1.89	64.4
3	**Ni1**	40	400 : 1	1.47	3.47	1.45	54.8
4	**Ni1**	50	400 : 1	1.36	3.09	1.40	41.3
5	**Ni1**	30	300 : 1	0.32	6.81	1.81	71.3
6	**Ni1**	30	500 : 1	1.94	5.32	2.02	62.9
7	**Ni1**	30	600 : 1	2.03	5.93	1.75	61.3
8	**Ni1**	30	700 : 1	1.79	4.69	1.91	61.2
9	**Ni2**	30	600 : 1	1.15	4.89	1.83	61.0
10[e]	**Ni3**	30	600 : 1	1.64	5.67	1.92	72.6
11	**Ni4**	30	600 : 1	3.83	11.1	1.94	90.4
12	**Ni5**	30	600 : 1	4.17	13.7	2.07	104.1
13	**Ni6**	30	600 : 1	1.89	15.4	2.41	117.8

[a] Conditions: 2.0 μmol of nickel precatalyst, 100 mL of toluene, 10 atm C_2H_4, 30 °C, 30 min. [b] Values in units of 10^6 g (mol of Ni)$^{-1}$ h^{-1}. [c] M_w in units of kg mol^{-1}, determined by GPC. [d] Determined by DSC. [e] The results for **Ni3** are consistent with the published data.[30]

substituents generally showed higher activities compared to those bearing electron-donating substituents. Indeed, the highest activity was observed using CF_3-containing **Ni5** (4.17 × 10^6 g of PE (mol of Ni)$^{-1}$ h^{-1}, run 12, Table 2). It remains unclear as to why NO_2-containing **Ni6** does not follow this trend, but related phenomenon have also been observed in other catalyst systems containing NO_2 substituents.[32,33,38] When compared to CF_3, the NO_2 substituent exhibits stronger electron-withdrawing ability, as is evidenced by the Hammett constants ($\sigma_p(NO_2)$ = 0.78, $\sigma_p(CF_3)$ = 0.56).[39] However, NO_2 not only displays strong electron-withdrawing ability, but is also a highly reactive unit.[40] Hence, in the presence of excess of the [Al] activators, side reactions may occur, resulting in decreased activity. As a further observation, there is a tendency for the molecular weight and T_m values of the PE to increase as the electron-withdrawing properties of the *para*-R group increase with NO_2-containing **Ni6** producing the highest M_w of 15.4 kg mol^{-1}. It would seem likely that the enhanced electrophilicity of the active metal centre facilitates the chain propagation leading to higher activity and higher molecular weight polymer.

To explore the branching density of the polymers produced using **Ni1**–**Ni6** in runs 7 and 9–13 (Table 2), we used semi-quantitative high temperature ^{13}C NMR spectroscopy to measure it.[17,41–44] Table 3 collects together the results of the data analysis along with the values of the branching density (B) expressed in terms of branches per 1000 Cs. As shown in Table 3, the BPE produced by this catalyst family displays a medium to high degree of branching, with levels falling between 61 and 99/1000 Cs. Evidently, as the *para*-R substituent changes from electron-donating to electron-withdrawing, the branching density tends to decrease. This result is consistent with that reported by Long and Chen,[32,33] where the nickel complexes bearing electron-withdrawing substituents tend to decrease the branching density. This trend may be explained by the competition between the various steps in the ethylene polymerisation process. In *N*,*N*-nickel catalyst systems, the competition between chain-walking and chain propagation determines the preference of branch formation.[43,45–50] This can be further rationalised in term of the ability of their β-agostic intermediates to undergo ethylene coordination. Where the electron withdrawing substituents increase the electron deficiency at the nickel centre, thereby promoting the ethylene coordination over chain walking.[43,45,47,49,51,52]

All BPEs producing **Ni1**–**Ni6** with EASC as activator were further investigated using ^{13}C NMR spectroscopy. The ^{13}C NMR spectrum of the polymer produced using **Ni1**/EASC (run 7, Table 2) is shown as a representative example in Fig. 2 (PE-**Ni1**), while others are included in the SI. The

Table 3 Branching density (B) and composition of the polymer samples[a,b]

		Branching composition (%)							
PE sample	B/1000 Cs	Me	Et	Pr	Bu	Amyl	Longer	Me (1,4-paired)	Me (1,6-paired)
PE-**Ni1**	99	79.8	0.2	4.6	2.1	4.1	9.2	5.3	5.5
PE-**Ni2**	98	81.1	1.3	0	5.2	0	12.5	3.6	6.0
PE-**Ni3**[c]	91	70.4	2.0	2.9	2.2	12.2	10.3	7.6	4.2
PE-**Ni4**	76	88.7	0	0	0	0	11.3	0	0
PE-**Ni5**	65	78.3	0	0	0	0	21.7	7.2	0
PE-**Ni6**	61	85.9	0	4.5	3.1	0	6.5	0	3.1

[a] Data obtained using high temperature ^{13}C NMR spectroscopy. [b] Analysis performed using approaches described in the literature.[41,43,44] [c] Data obtained from ref. 30.

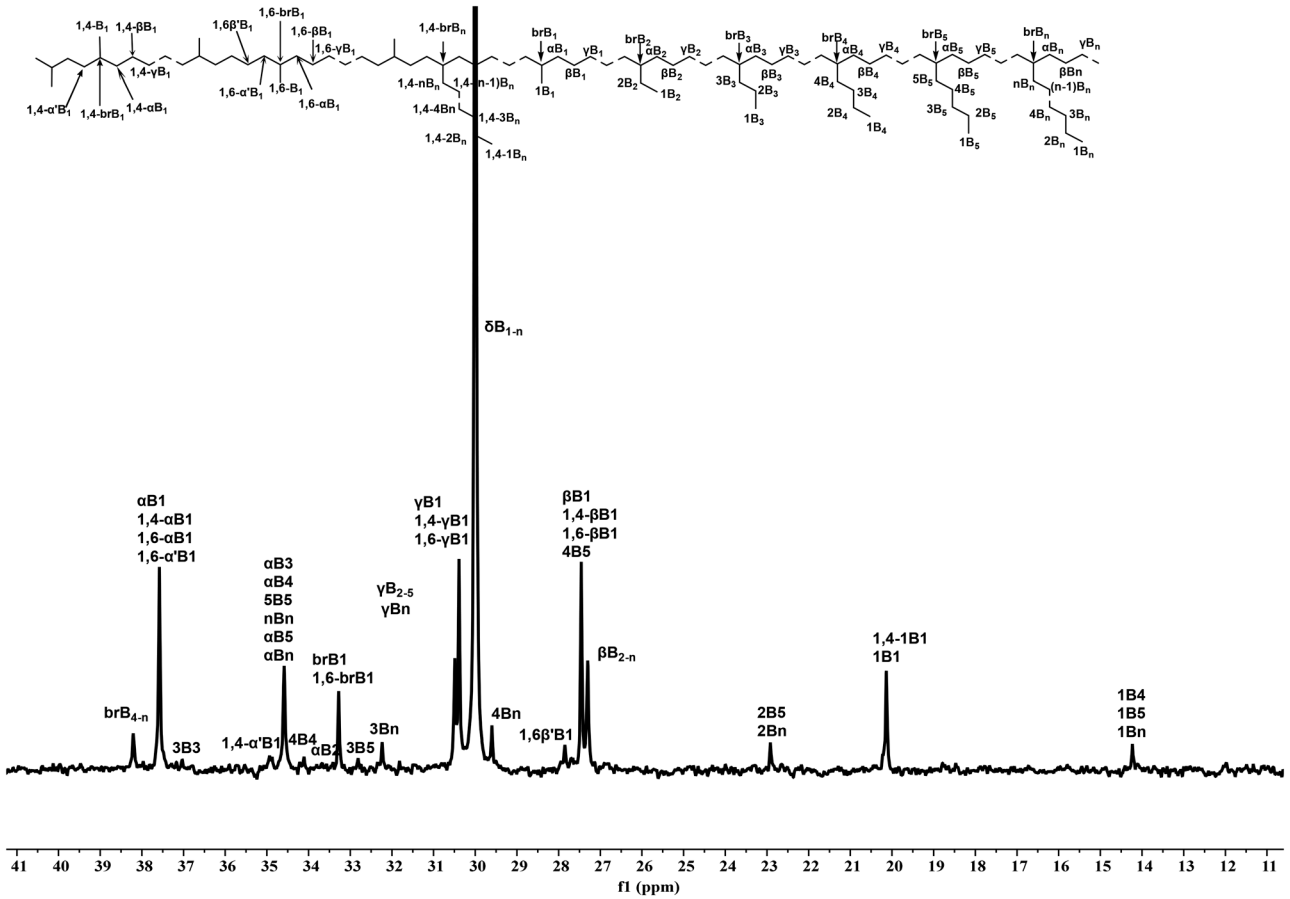

Fig. 2 ^{13}C NMR spectrum of PE-**Ni1** produced using **Ni1**/EASC (run 7, Table 2) in the region δ 11–41 ppm; recorded in $C_2D_2Cl_4$ at 100 °C.

upfield resonances seen between δ 10 to 40 ppm highlight the range of branching found in PE-**Ni1**. Analysis of these peaks reveals the presence of predominantly methyl branches, accounting for between 70–89% of the total branches, which may be attributed to the secondary carbons formed by chain-walking.[43] In contrast, other shorter chain branches are relatively scarce, with longer chain branches becoming more prevalent. Interestingly, for PE-**Ni4** and PE-**Ni5**, only methyl and longer branches were observed.

To more accurately discuss the influence of electronic effects of the catalysts on the polymerisation, it is necessary to introduce some parameters that can quantitatively describe the electronic properties. Herein, we make use of classical Hammett constants as well as the half-wave

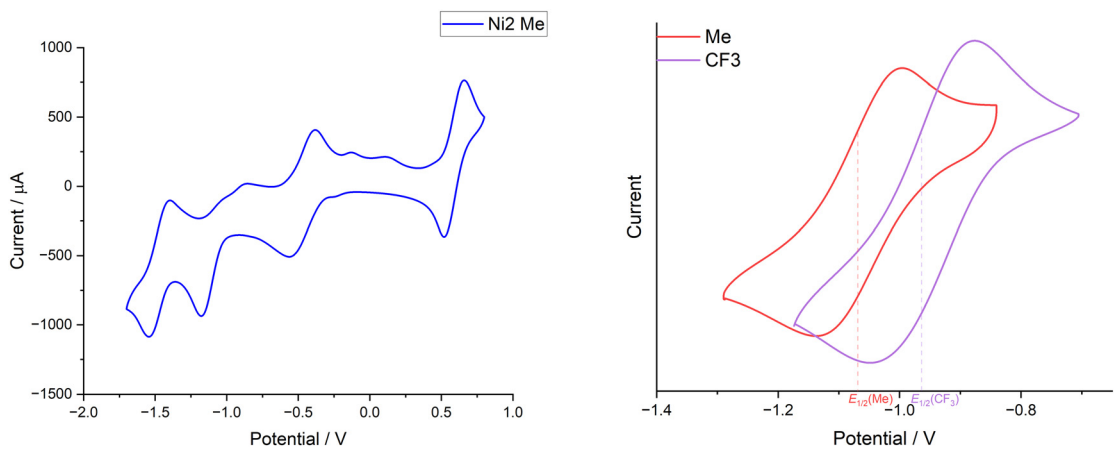

Fig. 3 Left: The CV trace for the global scan of **Ni2** (referenced to ferrocene/ferrocenium) in the region from −2.0 to 1.0 V. Right: The CV traces for the local scans of **Ni2** (Me) and **Ni5** (CF_3) in the region from −0.7 to −1.4 V.

potential in the discussion of the polymerisation results (*vide infra*).

(c) CV scans and $E_{1/2}$ measurements

In an attempt to correlate the distinct electronic properties of **Ni1**–**Ni6** with the variations in branching density as well as other properties of the polymer, we set about determining their half-wave potentials ($E_{1/2}$) by cyclic voltammetry (CV). Typically, these CV measurements were conducted using acetonitrile as the solvent, [nBu$_4$N][PF$_6$] as the supporting electrolyte and the scan rate fixed at 50 mV s^{-1}; all are referenced to a ferrocene/ferrocenium standard. Two representative local traces for **Ni2** and **Ni5** are shown in Fig. 3(right), along with the global scan for **Ni2** (Fig. 3, left); all other global and local scans for the nickel complexes are collected in the SI. The $E_{1/2}$ values were determined from the average value of the oxidative and reductive peak potentials of the quasi-reversible peak in the CV traces.[53]

For **Ni2** (Me) and **Ni5** (CF$_3$), the differences in the magnitude of the $E_{1/2}$ values of −1.057 V and −0.963 V, respectively, show how the nature of the *para*-R group impacts on this parameter. Specifically, the more electron-withdrawing the group is, the less negative the value of $E_{1/2}$. For purposes of comparison, these $E_{1/2}$ values for all six complexes are collected alongside the Hammett constants[39] for the given R groups in Table 4, and are additionally plotted in Fig. 4. Inspection of the plot, reveals a R^2 value of 0.99 implying a highly linear correlation between the σ_p for the *para*-R substituent and the $E_{1/2}$ of the nickel precatalyst. In addition, the complexes bearing electron-donating groups exhibit lower σ_p and $E_{1/2}$. It is worth noting that whilst the Hammett constant provides an electronic effect of the particular substituent, it does not comprehensively account for the behaviour of the entire complex. Nevertheless, the two parameters indicate excellent correlation within the error bars.

By inspection of Table 4, two key points emerge. Firstly, the branching density of the polymer generally shows a downward trend as the $E_{1/2}$ value becomes less negative; this data is plotted in Fig. 5. Evidently, the $E_{1/2}$ and branching

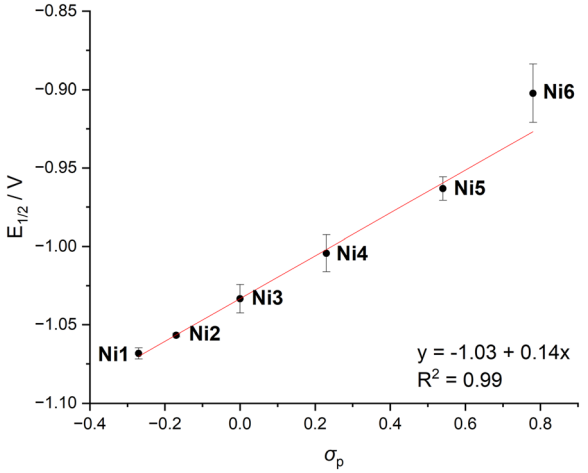

Fig. 4 Plot of experimentally determined $E_{1/2}$ values against the Hammett constants (σ_p) of the *para*-R groups in the nickel precatalysts (R^2 = 0.99).

density (B) exhibited a linear negative correlation, which can be fitted into a linear function $E_{1/2}$ = −0.7–0.004B, where the R^2 = 0.96 demonstrated a significant correlation. Notably, the slope indicates that for every 0.01 V difference in $E_{1/2}$, a change of around 3 branches/1000 Cs occurs in the resulting BPE. Furthermore, it can also be observed that for catalysts bearing electron withdrawing groups (NO$_2$, CF$_3$, Br), the branching density decreases with appreciable changes in $E_{1/2}$. By contrast, for catalysts bearing electron donating groups (MeO, Me), the variation in $E_{1/2}$ is less pronounced, with only minor changes in the distinctly higher values of B. As mentioned earlier, we attribute this increased branching to the decreasing electrophilicity of the active metal centre leading to more favourable chain-walking over chain propagation. Nevertheless, these result point towards the possibility that the value of $E_{1/2}$ could be used as predictive tool to measure branching density without the need for

Table 4 $E_{1/2}$ values for the nickel precatalysts, Hammett constants for their R groups and selected polymer data

	Ni1	Ni2	Ni3	Ni4	Ni5	Ni6
para-R	OMe	Me	H	Br	CF$_3$	NO$_2$
$E_{1/2}$[a] (V)	−1.068	−1.057	−1.033	−1.004	−0.963	−0.902
σ_p[b]	−0.27	−0.17	0	0.23	0.54	0.78
M_w[c]	5.93	4.89	5.67	11.1	13.7	15.4
B[d]	99	98	91	76	65	61
T_m[e]	61.3	61.0	72.6	90.4	104.1	117.8

[a] Half-wave potential of the nickel complexes determined from their cyclic voltammograms. [b] Hammett values obtained from the literature.[39] [c] M_w in units of kg mol^{-1}. [d] B = branches per 1000 Cs. [e] Melting temperature in units of °C.

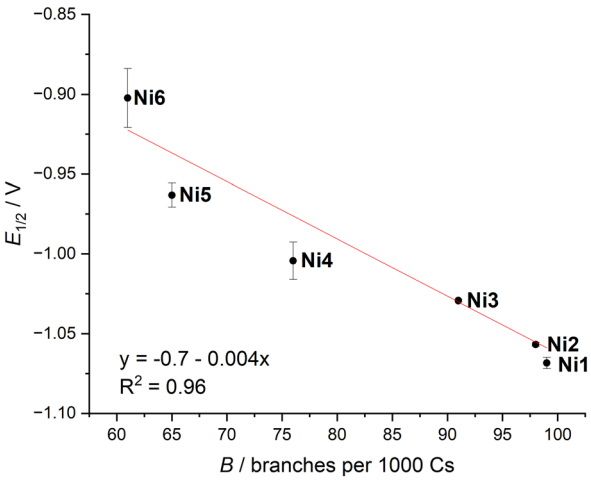

Fig. 5 Plot of experimentally determined $E_{1/2}$ values (in V) against the experimental branching density B (R^2 = 0.96).

additional polymerisation tests. This hypothesis has been previously proposed and tested by Long *et al.*[33] using the classic Brookhart type α-diimine nickel catalyst. In this work, we have extended this to the 2-iminopyridine-nickel catalyst family where we have broadened the range of substituents, and noted comparable observations.

As a second point, the variation in $E_{1/2}$ can also, to some degree, be correlated with the molecular weight of the BPE. As shown in Fig. 6, the $E_{1/2}$ and the M_w of the polymer formed by the nickel catalysts followed a positive linear trend with an R^2 = 0.89. However, it is evident for catalysts bearing electron withdrawing groups this relationship works well but is less effective with electron donating groups. In the latter case, the polymer molecular weights do not increase sequentially with $E_{1/2}$ for **Ni1** (OMe) and **Ni2** (Me) displaying minimal variations and comparable with **Ni3** (H). These findings are consistent with previous reports using a similar catalyst type.[30] However, the introduction of electron withdrawing groups in **Ni4**–**Ni6** sees the M_w increase steadily within the 10^4 kg mol^{-1} range with $E_{1/2}$. Indeed, the highest molecular weight BPE was found in **Ni6**/EASC, 15.4 kg mol^{-1}, which is significantly higher (3–5 times) than in previous reported results.[30,54,55] To the knowledge of the authors, this trend has not been observed in other 2-iminopyridine-nickel catalysts where electronic modifications have been made to the *N*-aryl group.[30] It is likely that this can be attributed to the more direct and enhanced electronic effect on the nickel centre by the *para*-R substitution of the conjugated pyridine ring.

Conclusions

In summary, a novel family of 2-(arylimino)-4-R-pyridine-nickel(II) precatalysts, **Ni1**–**Ni6**, differing only in their electronic properties of the 4-R group (R = OMe, Me, H, Br, CF_3, NO_2), has been successfully synthesised in good to high yield. Structural characterisation, performed on **Ni1**–**Ni6** highlights the significant steric properties imparted by the *ortho*-di(4-fluoro)benzhydryl groups and the impact the *para*-R group have on key bond parameters. On activation with EASC, all catalysts displayed high activity producing branched polymers with narrow dispersity. The highest catalyst activity was obtained with CF_3-containing **Ni5** while NO_2-containing **Ni6** produced the highest molecular weight and least branched polyethylene (15.4 kg mol^{-1}; 61 branches/1000 Cs). Cyclic voltammetry has been performed on **Ni1**–**Ni6** and has allowed $E_{1/2}$ values to be readily extracted. These $E_{1/2}$ values vary depending on the type of 4-R substituent, and show strong correlation with their Hammett constant. Moreover, it is evident that the value of $E_{1/2}$ can be correlated with not only the branching density but also to some level the molecular weight of the resulting polymer. In particular, as the $E_{1/2}$ of the complex becomes more negative, the branching density increases. Overall, we feel these observations support the concept that the value of $E_{1/2}$ for a nickel precatalyst shows promise as a tool for predicting the level of branching, and in all likelihood other polymer properties such as molecular weight. More generally, this methodology has scope to provide a valuable insight for producing BPE's with specific properties for a given application.

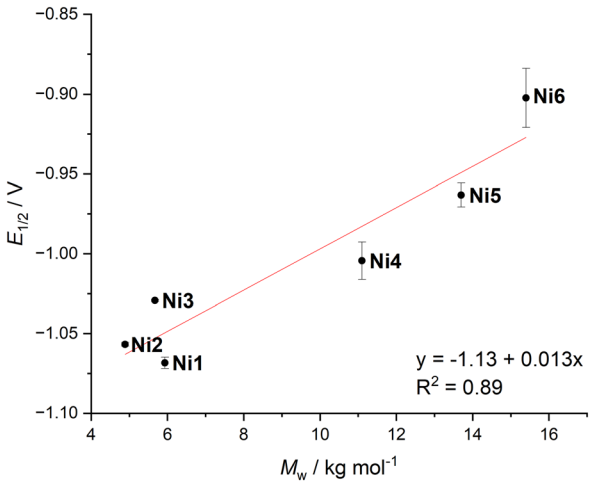

Fig. 6 Plot of experimentally determined $E_{1/2}$ values (in V) against molecular weight of the PE's produced by **Ni1**–**Ni6** (R^2 = 0.89).

Experimental section

(a) Materials and methods

All air-sensitive experiments were carried out under a nitrogen atmosphere using standard Schlenk techniques. Deuterated solvents used for NMR analysis were pre-dried. All solvents were dried over the appropriate drying agent and distilled under nitrogen where necessary. All NMR spectra data (^{1}H, ^{13}C, ^{19}F) were recorded on a Bruker Avance III 500 MHz spectrometer with a 5 mm BBO probe, Bruker Avance III HD 400 MHz spectrometer with a 5 mm BBO probe or a Bruker Avance NEO 500 MHz spectrometer with either a 5 mm Prodigy BBO cryoprobe or a 5 mm BBFO probe in the deuterated solvents $CDCl_3$ or CD_3OD. The determination of the magnetic moments (μ_{eff}) for the nickel(II) complexes made use of the Evans NMR method described previously.[36] Infra-red (IR) data were recorded using a Perkin Elmer Spectrum One instrument in the solid state. Elemental analysis was recorded on a Flash EA 1112 microanalyzer. Electrospray ionisation mass spectrometry analyses were completed in acetonitrile using a Waters Quattro mass spectrometer with a Gilson HPLC system included, as well as a Waters SQD2 mass spectrometer with a Waters Acquity H-Class UPLC and Waters 2777C Auto-sampler included. The GPC data was recorded on a PL-GPC220 instrument operating at 150 °C with 1,2,4-trichlorobenzene as the solvent at a flow rate of 1.0 mL min^{-1}. The DSC data was recorded on a PerkinElmer TA-Q2000 DSC analyser under a nitrogen atmosphere. During this procedure, a sample (4.0–6.0 mg) was heated to 150 °C at a rate of 20 °C min^{-1} and kept for 5 min at 150 °C to remove the thermal history and cooled to

−20 °C at a rate of 20 °C min^{-1}. For the ^{13}C NMR spectra of the polyethylenes, a weighed amount of polyethylene (*ca.* 50 mg) was added to 1,1,2,2-tetrachloroethane-d_2 (1 mL) with TMS as an internal standard. Inverse gated ^{13}C spectra recorded on a Bruker AV III 500WB spectrometer at 100 °C in 5 mm standard glass tubes at 100 °C with the number of scans between 3537 and 4352. Operating conditions used: spectral width 17 986 kHz; acquisition time 1.8 s; relaxation delay 2.0 s; pulse width 15.5 μs. An estimation of the branching content was made by integration of the corresponding peaks in the ^{13}C NMR spectra using approaches described in the literature.[42,44] Cyclic voltammetry measurements were conducted using a potentiostat with 0.01 mmol of the nickel complexes dissolved in 3 mL of dry acetonitrile containing a supporting electrolyte of 0.2 M nBu_4NPF_6. A silver electrode was used as the reference electrode, a platinum working electrode, and a platinum counter electrode. The measurements were performed at a scan rate of 50 mV s^{-1}.

All chemicals used in the experiments were sourced from commercial suppliers, unless otherwise specified for synthetic chemicals. Full synthetic details for 2-(arylimino)-4-R-pyridines, 2-{(2,6-{(p-FC_6H_4)$_2$CH}$_2$-4-MeC_6H_2)N=CMe}-4-RC_5H_3N (**L1** R = OMe, **L2** R = Me, **L3** R = H, **L4** R = Br, **L5** R = CF_3, **L6** R = NO_2) are presented in the SI.

(b) Syntheses of the nickel(II) complexes

L1NiBr$_2$ (Ni1). A small dry Schlenk flask equipped with a magnetic stirrer was evacuated and backfilled with nitrogen. $NiBr_2$(DME) (0.031 g, 0.10 mmol) and dry CH_2Cl_2 (10 mL) were added, and the reaction mixture was stirred at room temperature until almost all the nickel salt had dissolved. **L1** (0.065 g, 0.1 mmol) was added and the mixture was stirred at room temperature overnight. At the end of the reaction, petroleum ether 40/60 (50 mL) was added and the resulting precipitate was allowed to settle to the bottom. The supernatant solution was removed by syringe and the precipitate was washed with petroleum ether (2 × 50 mL). Following drying under reduced pressure, **Ni1** was isolated as a green solid (0.06 g, 70%). Table S1 gives the ^1H NMR data. ^{19}F NMR (500 MHz, $CDCl_3$): δ ppm −115.42, −116.80. ESMS (MeCN) m/z: 783 [M–Br], 824 [M–Br + MeCN]. FT-IR (cm^{-1}): 1013 (w), 1040 (m), 1098 (w), 1157 (s), 1219 (s), 1324 (s), 1503 (s), 1603 (m, C=N), 2362 (w), 2980 (w). Anal. Calcd. for $C_{41}H_{32}Br_2F_4N_2NiO$·MeCN·1/4$CH_2Cl_2$: C 56.13, H 3.87, N 4.54; found C 56.30, H 3.52, N 4.77. μ_{eff} (Evans NMR): 2.92 BM.

L2NiBr$_2$ (Ni2). Ni2 was prepared using a similar method and molar ratios as that described for **Ni1** and was isolated as a green solid (0.073 g, 82%). Table S1 gives the ^1H NMR data. ^{19}F NMR (500 MHz, $CDCl_3$): δ ppm −114.99, −116.32. ESMS (MeCN) m/z: 767 [M–Br]. FT-IR (cm^{-1}): 1013 (w), 1028 (w), 1098 (w), 1157 (m), 1217 (s), 1320 (w), 1374 (w), 1503 (s), 1546 (w), 1606 (m, C=N), 2924 (w), 2982 (w), 3056 (w). Anal. Calcd. for $C_{41}H_{32}Br_2F_4N_2Ni$·1.5MeCN·0.5H_2O: C 57.58, H 4.12, N 5.34; found C 57.74, H 4.14, N 5.44. μ_{eff} (Evans NMR): 2.68 BM.

L3NiBr$_2$ (Ni3). Ni3 was prepared using a similar method and molar ratios as that described for **Ni1** and was isolated as a green solid (0.102 g, 83%). The IR data and ^{19}F NMR data are consistent with what has been previously reported.[30] Table S1 gives the ^1H NMR data. μ_{eff} (Evans NMR): 2.78 BM.

L4NiBr$_2$ (Ni4). Ni4 was prepared using a similar method and molar ratios as that described for **Ni1** and was isolated as a green solid (0.12 g, 67%). Table S1 gives the ^1H NMR data. ^{19}F NMR (500 MHz, $CDCl_3$): δ ppm −114.99, −116.32. ESMS (MeCN) m/z: 797 [M–2Br + H + MeCN], 832 [M–Br], 872 [M–Br + MeCN]. FT-IR (cm^{-1}): 1015 (w), 1095 (w), 1157 (m), 1217 (s), 1311 (m), 1503 (s), 1577 (w), 1600 (w, C=N), 2926 (w), 3054 (w), 3074 (w). Anal. Calcd. for $C_{42}H_{32}Br_3F_4N_3Ni$·3/2MeCN: C 53.04, H 3.47, N 5.04; found C 53.13, H 3.51, N 5.18. μ_{eff} (Evans NMR): 2.64 BM.

L5NiBr$_2$ (Ni5). A small dry Schlenk flask equipped with a magnetic stirrer was evacuated and backfilled with nitrogen. $NiBr_2$(DME) (0.031 g, 0.1 mmol) and dry CH_2Cl_2 (8 mL) and dry EtOH (2 mL) were added, and the reaction mixture was stirred at room temperature until all the nickel salt had dissolved. **L5** (0.066 g, 0.1 mmol) was added and the mixture was stirred at room temperature overnight. Upon completion, the solvent was removed under reduced pressure. The solid was wash with diethyl ether and hexane, **Ni5** was isolated as a green solid (0.078 g, 89%). Table S1 gives the ^1H NMR data. ^{19}F NMR (500 MHz, $CDCl_3$): δ ppm −64.65, −114.46, −116.31. ESMS (MeCN) m/z: FT-IR (cm^{-1}): 1015 (w), 1087 (w), 1155 (m), 1184 (m), 1223 (m), 1264 (m), 1307 (w), 1339 (w), 1374 (w), 1423 (w), 1503 (s), 1602 (w, C=N), 2922 (w) Anal. Calcd. for $C_{41}H_{29}Br_2F_7N_2Ni$: C 54.64, H 3.24, N 3.11; found C 54.30, H 3.30, N 2.95. μ_{eff} (Evans NMR): 3.05 BM.

L6NiBr$_2$ (Ni6). Ni6 was prepared using a similar method and molar ratios as that described for **Ni5** and was isolated as a green solid (0.055 g, 60%). Table S1 gives the ^1H NMR data. ^{19}F NMR (500 MHz, $CDCl_3$): δ ppm −114.12, −116.09. ESMS (MeCN) m/z: 798 [M–Br], 840 [M–Br + MeCN]. FT-IR (cm^{-1}): 1015 (w), 1095 (w), 1157 (m), 1225 (s), 1315 (w), 1355 (w), 1505 (s), 1540 (w), 1600 (w, C=N), 2852 (w), 2920 (w). Anal. Calcd. for $C_{40}H_{29}Br_2F_4N_3NiO_2$·3/2EtOH·1/4$CH_2Cl_2$: C 53.64, H 4.34, N 4.01; found C 53.62, H 4.08, N 4.16. μ_{eff} (Evans NMR): 2.98 BM.

(c) Ethylene polymerisation evaluation

The polymerisation runs were carried out in a stainless-steel autoclave (250 mL) which was equipped with an ethylene pressure control system, a temperature controller and a mechanical stirrer. The precatalyst (2 μmol) was added to an oven-dried autoclave, which was then placed under reduced pressure and backfilled with ethylene three times. When the set reaction temperature was reached, freshly distilled toluene (3 × 25 mL) was injected into the autoclave to dissolve the precatalyst. The required amount of activator

(*i.e.*, MAO, MMAO, $EtAlCl_2$, Et_2AlCl, EASC) was introduced by syringe followed by more toluene (25 mL) to complete the addition. The autoclave was immediately pressurised to 10 atm of C_2H_4, and the mechanical stirring commenced. After the required reaction time, the autoclave was allowed to cool to room temperature and the ethylene pressure released before 10% hydrochloric acid in ethanol added to quench the reaction. The polymer was collected by filtration and washed with ethanol. Following drying under at room temperature overnight, the polymer sample was weighed.

(d) Crystallographic determinations

Data for **Ni1**–**Ni6** were collected using a Bruker D8 Quest diffractometer with a Photon III detector and a microfocus source with Cu-Kα radiation (λ = 1.54178). Intensities were integrated from data recorded on 1° frames by ω or φ rotation. A multi-scan method absorption correction was applied. The structures were solved using SHELXS or SHELXT the datasets were refined by full-matrix least-squares on reflections with $F^2 \geq 2\sigma(F^2)$ values, with anisotropic displacement parameters for all nonhydrogen atoms, and with constrained riding hydrogen geometries; U_{iso}(H) was set at 1.2 (1.5 for methyl groups) times U_{eq} of the parent atom. SHELX was employed through OLEX2(1) for structure solution and refinement.[56] Crystal data and crystallographic parameters for all six structures are summarised in Table S2.

Author contributions

Y. Z. led the design of experiments, data collection and analysis, and writing – original draft, K. S. contributed to XRD analysis, Y. W. contributed to polymer analysis, W.-H. S. contributed to supervision, and G. A. S. contributed to supervision, conceptualisation, methodology, review and editing.

Conflicts of interest

There are no conflicts to declare.

Data availability

Figures, additional characterisation data for the nickel complexes, polymers and CV studies. See DOI: **https://doi.org/10.1039/D5CY00859J**.

The data supporting this article have been included as part of the SI. Crystallographic data for **Ni1**–**Ni6** have been deposited at the CCDC under 2469276–2469281 and can be obtained from **https://ccdc.cam.ac.uk**.

Acknowledgements

Y. Z. thanks the China Scholarship Council for financial support and the Chinese Academy of Science for a short-term visiting position. G. A. S. is grateful to the Chinese Academy of Sciences President's International Fellowship Initiative (Grant No. 2025PVB0034). The EPSRC are acknowledged for grant EP/W02151X/1.

References

1 D. Sauter, M. Taoufik and C. Boisson, Polyolefins, a Success Story, *Polymer*, 2017, **9**, 185.
2 P. Galli and G. Vecellio, Polyolefins: The most promising large-volume materials for the 21st century, *J. Polym. Sci., Part A: Polym. Chem.*, 2004, **42**, 396–415.
3 P. D. Hustad, Frontiers in Olefin Polymerization: Reinventing the World's Most Common Synthetic Polymers, *Science*, 2009, **325**, 704–707.
4 R. Wu, W. K. Wu, L. Stieglitz, S. Gaan, B. Rieger and M. Heuberger, Recent advances on α-diimine Ni and Pd complexes for catalyzed ethylene (Co)polymerization: A comprehensive review, *Coord. Chem. Rev.*, 2023, **474**, 214844.
5 Z. Wang, Q. Liu, G. A. Solan and W.-H. Sun, Recent advances in Ni-mediated ethylene chain growth: *N*imine-donor ligand effects on catalytic activity, thermal stability and oligo-/polymer structure, *Coord. Chem. Rev.*, 2017, **350**, 68–83.
6 Y. Na, S. Dai and C. Chen, Direct Synthesis of Polar-Functionalized Linear Low-Density Polyethylene (LLDPE) and Low-Density Polyethylene (LDPE), *Macromolecules*, 2018, **51**, 4040–4048.
7 H. Suo, I. V. Oleynik, C. Huang, I. I. Oleynik, G. A. Solan, Y. Ma, T. Liang and W.-H. Sun, *ortho*-Cycloalkyl substituted *N*, *N*′-diaryliminoacenaphthene-Ni(II) catalysts for polyethylene elastomers; exploring ring size and temperature effects, *Dalton Trans.*, 2017, **46**, 15684–15697.
8 G. Zanchin and G. Leone, Polyolefin thermoplastic elastomers from polymerization catalysis: Advantages, pitfalls and future challenges, *Prog. Polym. Sci.*, 2021, **113**, 101342.
9 R. M. Patel, P. Jain, B. Story and S. Chum, in *Innovations in Industrial and Engineering Chemistry*, American Chemical Society, 2008, vol. 1000, pp. 71–102.
10 J. Gan and S. Dai, Synthesis of high MFI polyolefin elastomers using dibenzosuberyl iminopyridyl Ni(II) catalysts, *Polym. Chem.*, 2025, **16**, 3172–3179.
11 Q. Mahmood, Z. Hu, G. Ren and W.-H. Sun, Recent advances in nickel Catalysis for thermoplastic polyethylene elastomers: Synthesis strategies, properties, and future perspectives, *Coord. Chem. Rev.*, 2025, **541**, 216833.
12 D. Zhu, D. Jia, Q. Zhang, Y. Ma, Q. Mahmood and W.-H. Sun, Tuning 2,3-Bis(arylimino)butane-nickel Precatalysts for High-Molecular-Weight Polyethylene Elastomers, *Molecules*, 1847, **2025**, 30.
13 A. M. Ashfaq, Q. Zhang, Y. Wang, Y. Ma, Q. Xing, M. Sun, T. Liang and W.-H. Sun, Thermostable polyhalogen-substituted α-diimine nickel precatalysts towards high performance polyethylene elastomer, *J. Mol. Struct.*, 2025, **1334**, 141892.
14 A. Khalid, Z. Hu, Y. Ma, Q. Mahmood, G. Ren, A. Razzaq, Y. Wang, T. Liang and W.-H. Sun, Benzosuberyl-congested asymmetrical α-diiminonickel halides for achieving methyl-

branched polyethylenes with tunable plastic to elastomeric properties, *Eur. Polym. J.*, 2025, **223**, 113635.
15 H. Saeed, Q. Mahmood, R. Yuan, Y. Wang, S. Zou, K. F. Tahir, Y. Ma, T. Liang and W.-H. Sun, High-performance polyethylene elastomers using a hybrid steric approach in α-diimine nickel precatalysts, *Polym. Chem.*, 2024, **15**, 1437–1452.
16 E. Y.-X. Chen, Coordination Polymerization of Polar Vinyl Monomers by Single-Site Metal Catalysts, *Chem. Rev.*, 2009, **109**, 5157–5214.
17 M. F. Llauro, C. Monnet, F. Barbotin, V. Monteil, R. Spitz and C. Boisson, Investigation of Ethylene/Butadiene Copolymers Microstructure by ^{1}H and ^{13}C NMR, *Macromolecules*, 2001, **34**, 6304–6311.
18 H. J. Lee, J. W. Baek, T. J. Kim, H. S. Park, S. H. Moon, K. L. Park, S. M. Bae, J. Park and B. Y. Lee, Synthesis of Long-Chain Branched Polyolefins by Coordinative Chain Transfer Polymerization, *Macromolecules*, 2019, **52**, 9311–9320.
19 S. Mecking, L. K. Johnson, L. Wang and M. Brookhart, Mechanistic Studies of the Palladium-Catalyzed Copolymerization of Ethylene and α-Olefins with Methyl Acrylate, *J. Am. Chem. Soc.*, 1998, **120**, 888–899.
20 L. K. Johnson, C. M. Killian and M. Brookhart, New Pd(II)- and Ni(II)-Based Catalysts for Polymerization of Ethylene and alpha-Olefins, *J. Am. Chem. Soc.*, 1995, **117**, 6414–6415.
21 T. V. Laine, U. Piironen, K. Lappalainen, M. Klinga, E. Aitola and M. Leskelä, Pyridinylimine-based nickel(II) and palladium(II) complexes: preparation, structural characterization and use as alkene polymerization catalysts, *J. Organomet. Chem.*, 2000, **606**, 112–124.
22 G. J. P. Britovsek, S. P. D. Baugh, O. Hoarau, V. C. Gibson, D. F. Wass, A. J. P. White and D. J. Williams, The role of bulky substituents in the polymerization of ethylene using late transition metal catalysts: a comparative study of nickel and iron catalyst systems, *Inorg. Chim. Acta*, 2003, **345**, 279–291.
23 R. Gao, W.-H. Sun and C. Redshaw, Nickel complex pre-catalysts in ethylene polymerization: new approaches to elastomeric materials, *Catal. Sci. Technol.*, 2013, **3**, 1172–1179.
24 S. Wang, W.-H. Sun and C. Redshaw, Recent progress on nickel-based systems for ethylene oligo−/polymerization catalysis, *J. Organomet. Chem.*, 2014, **751**, 717–741.
25 J. O. D. Williams, G. A. Solan, J. Xu, J. Allen, R. C. Harris and V. M. Timmermann, Investigating Branched Polyethylene Sensors for Applications in Prosthetics, *Macromol. Chem. Phys.*, 2021, **222**, 2100206.
26 M. Stürzel, S. Mihan and R. Mülhaupt, From Multisite Polymerization Catalysis to Sustainable Materials and All-Polyolefin Composites, *Chem. Rev.*, 2016, **116**, 1398–1433.
27 G. Dalla Fontana, R. Mossotti and A. Montarsolo, Assessment of microplastics release from polyester fabrics: The impact of different washing conditions, *Environ. Pollut.*, 2020, **264**, 113960.
28 Q. Mahmood, X. Li, L. Qin, L. Wang and W.-H. Sun, Structural evolution of iminopyridine support for nickel/palladium catalysts in ethylene (oligo)polymerization, *Dalton Trans.*, 2022, **51**, 14375–14407.
29 H. Liu, W. Zhao, X. Hao, C. Redshaw, W. Huang and W.-H. Sun, 2,6-Dibenzhydryl-N-(2-phenyliminoacenaphthylenylidene)-4-methylbenzenamine Nickel Dibromides: Synthesis, Characterization, and Ethylene Polymerization, *Organometallics*, 2011, **30**, 2418–2424.
30 Z. Hosseinzadeh, M. Liu, Q. Zhang, T. Liang, G. A. Solan, Y. Ma and W.-H. Sun, Electronic Tuning of Sterically Encumbered 2-(Arylimino)Pyridine-Nickel Ethylene Polymerization Catalysts by para-Group Modification, *Catalysts*, 2022, **12**, 1520.
31 L. Guo, S. Li, M. Ji, W. Sun, W. Liu, G. Li, J. Zhang, Z. Liu and S. Dai, Monoligated vs Bisligated Effect in Iminopyridyl Nickel Catalyzed Ethylene Polymerization, *Organometallics*, 2019, **38**, 2800–2806.
32 M. Chi, A. Chen, W. Pang, C. Tan and C. Chen, Positional Electronic Effects in Iminopyridine-*N*-oxide Nickel Catalyzed Ethylene Polymerization, *Chin. J. Chem.*, 2021, **39**, 1683–1689.
33 A. M. Doerr, M. R. Curry, R. C. Chapleski, J. M. Burroughs, E. K. Lander, S. Roy and B. K. Long, Redox Potential as a Predictor of Polyethylene Branching Using Nickel α-Diimine Catalysts, *ACS Catal.*, 2022, **12**, 73–81.
34 A. W. Addison, T. N. Rao, J. Reedijk, J. van Rijn and G. C. Verschoor, Synthesis, structure, and spectroscopic properties of copper(II) compounds containing nitrogen–sulphur donor ligands; the crystal and molecular structure of aqua[1,7-bis(*N*-methylbenzimidazol-2′-yl)-2,6-dithiaheptane]copper(II) perchlorate, *J. Chem. Soc., Dalton Trans.*, 1984, 1349–1356.
35 M. Shahid, G. Sanxaridou, S. Ottoboni, L. Lue and C. Price, Exploring the Role of Anti-solvent Effects during Washing on Active Pharmaceutical Ingredient Purity, *Org. Process Res. Dev.*, 2021, **25**, 969–981.
36 D. Ostfeld and I. A. Cohen, A cautionary note on the use of the Evans method for magnetic moments, *J. Chem. Educ.*, 1972, **49**, 829.
37 M. Lehr, T. Paschelke, E. Trumpf, A. Vogt, C. Näther, F. D. Sönnichsen and A. J. McConnell, A Paramagnetic NMR Spectroscopy Toolbox for the Characterisation of Paramagnetic/Spin-Crossover Coordination Complexes and Metal–Organic Cages, *Angew. Chem., Int. Ed.*, 2020, **59**, 19344–19351.
38 Q. Mahmood, Y. Zeng, X. Wang, Y. Sun and W.-H. Sun, Advancing polyethylene properties by incorporating NO_2 moiety in 1,2-bis(arylimino)acenaphthylnickel precatalysts: synthesis, characterization and ethylene polymerization, *Dalton Trans.*, 2017, **46**, 6934–6947.
39 C. Hansch, A. Leo and R. W. Taft, A survey of Hammett substituent constants and resonance and field parameters, *Chem. Rev.*, 1991, **91**, 165–195.
40 N. Apostolescu, T. Schröder and S. Kureti, Study on the mechanism of the reaction of NO_2 with aluminium oxide, *Appl. Catal., B*, 2004, **51**, 43–50.
41 P. M. Cotts, Z. Guan, E. McCord and S. McLain, Novel Branching Topology in Polyethylenes As Revealed by Light

Scattering and ^{13}C NMR, *Macromolecules*, 2000, **33**, 6945–6952.

42 G. B. Galland, R. F. de Souza, R. S. Mauler and F. F. Nunes, ^{13}C NMR Determination of the Composition of Linear Low-Density Polyethylene Obtained with [η^3-Methallyl-nickel-diimine]PF_6 Complex, *Macromolecules*, 1999, **32**, 1620–1625.

43 Y. Zhang, X. Kang and Z. Jian, Selective branch formation in ethylene polymerization to access precise ethylene-propylene copolymers, *Nat. Commun.*, 2022, **13**, 725.

44 G. B. Galland, R. Quijada, R. Rojas, G. Bazan and Z. J. A. Komon, NMR Study of Branched Polyethylenes Obtained with Combined Fe and Zr Catalysts, *Macromolecules*, 2002, **35**, 339–345.

45 L. Deng, P. Margl and T. Ziegler, A Density Functional Study of Nickel(II) Diimide Catalyzed Polymerization of Ethylene, *J. Am. Chem. Soc.*, 1997, **119**, 1094–1100.

46 D. G. Musaev, M. Svensson, K. Morokuma, S. Strömberg, K. Zetterberg and P. E. M. Siegbahn, Density Functional Study of the Mechanism of the Palladium(II)-Catalyzed Ethylene Polymerization Reaction, *Organometallics*, 1997, **16**, 1933–1945.

47 D. E. Ortega, D. Cortés-Arriagada, O. S. Trofymchuk, F. M. Nachtigall, L. S. Santos, R. S. Rojas and A. Toro-Labbé, Mechanistic study of the competitiveness between branched and linear polyethylene production on *N*-arylcyano-*β*-diketiminate nickel hydride, *Polym. Chem.*, 2020, **11**, 6640–6649.

48 D. G. Musaev, R. D. J. Froese and K. Morokuma, Molecular Orbital and IMOMM Studies of the Chain Transfer Mechanisms of the Diimine–M(II)-Catalyzed (M = Ni, Pd) Ethylene Polymerization Reaction, *Organometallics*, 1998, **17**, 1850–1860.

49 R. D. J. Froese, D. G. Musaev and K. Morokuma, Theoretical Study of Substituent Effects in the Diimine–M(II) Catalyzed Ethylene Polymerization Reaction Using the IMOMM Method, *J. Am. Chem. Soc.*, 1998, **120**, 1581–1587.

50 J. Ramos, V. Cruz, A. Muñoz-Escalona, S. Martínez and J. Martínez-Salazar, Computational studies of the Brookhart's type catalysts for ethylene polymerisation. Part 2: ethylene insertion and chain transfer mechanisms, *Polymer*, 2003, **44**, 2169–2176.

51 T. K. Woo and T. Ziegler, The influence of electronic and steric factors on chain branching in ethylene polymerization by Brookhart-type Ni(II) diimine catalysts: a combined density functional theory and molecular mechanics study, *J. Organomet. Chem.*, 1999, **591**, 204–213.

52 Z. Ye, J. Jiang, C. Zhao and Z. Ke, Deciphering Ligand Roles in Nickel-Catalyzed Polymerization of Ethylene: A DFT Study, *Macromolecules*, 2024, **57**, 11461–11475.

53 W. C. Anderson, S. H. Park, L. A. Brown, J. M. Kaiser and B. K. Long, Accessing multiple polyethylene grades via a single redox-active olefin polymerization catalyst, *Inorg. Chem. Front.*, 2017, **4**, 1108–1112.

54 X. Hou, T. Liang, W.-H. Sun, C. Redshaw and X. Chen, 2-Substituted 8-(2-benzhydrylarylimino)-5,6,7-trihydroquinoline-*N*,*N*′ nickel dichlorides: Synthesis, characterization and catalytic behavior towards ethylene, *J. Organomet. Chem.*, 2012, **708–709**, 98–105.

55 W.-H. Sun, S. Song, B. Li, C. Redshaw, X. Hao, Y.-S. Li and F. Wang, Ethylene polymerization by 2-iminopyridylnickel halide complexes: synthesis, characterization and catalytic influence of the benzhydryl group, *Dalton Trans.*, 2012, **41**, 11999.

56 O. V. Dolomanov, L. J. Bourhis, R. J. Gildea, J. A. K. Howard and H. Puschmann, OLEX2: a complete structure solution, refinement and analysis program, *J. Appl. Crystallogr.*, 2009, **42**, 339–341.